Journal of Materials Chemistry A

PAPER

View Article Online
View Journal

Cite this: DOI: 10.1039/c5ta08709k

Hierarchically porous BEA stannosilicates as unique catalysts for bulky ketone conversion and continuous operation†

Abbas Al-Nayili, Keiko Yakabi and Ceri Hammond*

Received 28th October 2015
Accepted 17th December 2015

DOI: 10.1039/c5ta08709k

www.rsc.org/MaterialsA

Pore size limitations typically limit the applicability of Lewis acidic zeolites, such as titano- and stannosilicates, to catalytic processes based on small-to-mid sized substrates, and increase their rates of deactivation, prohibiting further exploitation. Herein, we demonstrate that tin-containing zeolites possessing modified hierarchical BEA matrices can be prepared. These hierarchical stannosilicates are able to mediate the catalytic conversion of bulky ketone substrates, a pertaining challenge in the field that purely microporous analogues are unable to mediate. Deactivation studies in the continuous regime also demonstrate the exceptional stability of hierarchical Sn-Beta compared to purely microporous Sn-Beta, with <20% loss of activity observed over 700 h on stream. In contrast, the purely microporous analogue lost ±70% activity in only 200 h. To the best of our knowledge, this is the first time a stannosilicate with a beneficial hierarchical BEA framework has been prepared, and the first evidence of cyclododecanone valorisation with stannosilicate catalysts.

Introduction

Lewis acid catalysts have been widely used for a range of essential catalytic transformations, including biomass valorisation. Of particular interest are crystalline, porous inorganic materials such as zeolites, which contain encapsulated Lewis acidic centres, such as Al, Sn, Ti and Zr.[1–4] These materials combine the advantages of molecular catalysts, such as site isolation and high intrinsic activity, along with the practical advantages of heterogeneous catalysts, which simplify downstream processing. Amongst these materials, Sn-β, a medium pore zeolite possessing isolated Sn(IV) sites and BEA topology, has garnered tremendous levels of academic and industrial interest. Over the last decade, it has been demonstrated that this material possesses an exceptional ability to catalyse various transformations involving carbonyl compounds, such as the Baeyer–Villiger oxidation (BVO) of ketones,[5–7] the Meerwein–Pondorf–Verley (MPV) transfer hydrogenation of ketones to alcohols,[8–11] and the isomerization of renewable sugars such as glucose,[12–15] amongst several others.

In addition to high levels of activity, microporous crystalline zeolites, such as Sn-β, also provide excellent levels of hydrothermal stability, high surface area, and molecular sieving capability due to the uniform nature of their micropores. Possessing a microporous structure, Sn-β is, however, very susceptible to the limitations associated with this particular degree of confinement, such as (i) internal mass transfer limitations hindering catalytic performance through slow molecular diffusion, (ii) restricted diffusion of bulkier reactants, which limits their scope of reactivity, and (iii) increased rates of deactivation through pore blocking (*cf.* fouling). These limitations are, unfortunately, common to almost all microporous zeolites. Indeed, some of us recently demonstrated that despite exhibiting high levels of stability during steady state (continuous) operation, microporous Sn-β slowly deactivates with extended time on stream through fouling of the micropores with reaction products and higher molecular weight carbonaceous residue.[15]

Over the years, several approaches have been followed in order to alleviate these limitations, such as (i) the synthesis of extra-large pore zeolites,[17–19] (ii) the development of ordered mesoporous materials (*e.g.* MCM-41)[20] and related composites,[21] (iii) the preparation of nano-sized zeolite particles,[22] and (iv) the development of 2D materials.[23–28] Indeed, several of these approaches have been attempted for a range of zeotype materials, including silicates, aluminosilicate, titanosilicate, and more recently, stannosilicate. Nevertheless, each of these alternative materials experience particular disadvantages when it comes to catalytic activity, and several hurdles and challenges remain to be tackled. Decreased levels of specific active site activity (*e.g.* turnover frequency), poorer levels of hydrothermal stability and increased production costs (through the use of costly surfactant templates) are just three of the known disadvantages of each of the alternative materials that have been prepared to date.

Cardiff Catalysis Institute, Cardiff University, Main Building, Park Place, CF10 3AT, UK. E-mail: hammondc4@cardiff.ac.uk; Web: http://blogs.cardiff.ac.uk/hammond; Tel: +44 (0)29 2087 4082

† Electronic supplementary information (ESI) available. See DOI: 10.1039/c5ta08709k

Hierarchical zeolites are those that possess levels of mesoporosity imprinted upon the conventional microporous structure. In principle, these materials retain the advantages of purely microporous materials, such as increased intrinsic reactivity and (hydro)thermal stability, whilst also improving the particular disadvantages associated with overly confined materials, such as retarded diffusion and increased rates of deactivation.[29–31] Consequently, these materials have experienced an explosion of interest in recent years. Most of this attention has focused upon the generation of hierarchical aluminosilicate materials, unsurprising given their widespread use throughout the petrochemical industry.[32,33] Desilication, a top down approach involving the treatment of a parent zeolite in an alkaline medium under mild conditions, has been shown to be a particular efficient method of generating hierarchy.[34–36] The role of the base is to remove silicon atoms from the framework of the material (Fig. 1), thus resulting in partial destruction of the micropores, and leading to the appearance of mesoporosity. Under optimised conditions, this can lead to the generation of a hierarchical material without causing excessive destruction, *i.e.* collapse, of the zeolite framework.

Given their emerging status as sustainable heterogeneous catalysts, it is unsurprising that attention is being turned to the generation of stannosilicates with improved diffusional properties.[37–39] To date, however, focus has primarily been on the synthesis of stannosilicates with a hierarchical MFI-type topology, and very little attention[40] has been devoted to the synthesis of other hierarchical stannosilicates. Furthermore, in all of these previous cases, catalytic studies have only focused upon the conversion of relatively small substrates that do not present a significant hindrance for conventional medium pore zeolites, such as zeolite beta. Examples include the isomerisation of dihydroxyacetone (C_3) and the catalytic conversion of glucose (C_6). As such, full appreciation of the potential advantages of hierarchical stannosilicates has yet to be realised.

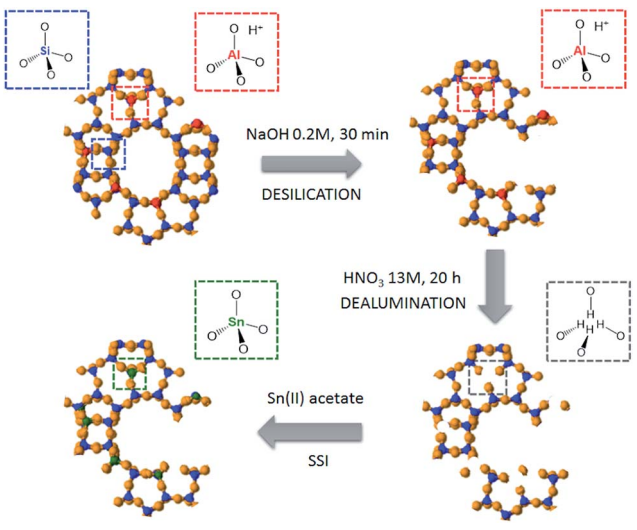

Fig. 1 Postsynthetic desilication procedure for mesopores creation in the zeolite β using NaOH as desilication agent (step 1), and subsequent formation of stannosilicate *via* solid state stannation (step 2 and 3).

Motivated by this research challenge, we demonstrate in this work that hierarchically-modified zeolite beta, doped with 2 wt% Sn through solid-state stannation, is an effective catalyst for the catalytic conversion of bulky ketones, such as cyclododecanone. These ketones are far too large to be catalytically converted in the micropores of even medium pore zeolites, and thus offer an ideal challenge for their hierarchical matrices. Kinetic and spectroscopic methodologies reveal that the active sites present in the hierarchical matrix are comparable to those found in the conventional microporous Sn-β despite the modified porosity, and that the hierarchical material demonstrates significantly higher levels of activity than ordered mesoporous analogues such as Sn-MCM-41. Furthermore, deactivation studies in continuous mode also demonstrate the supreme advantage of the hierarchical analogue when it comes to extended steady state operation, with high levels of activity observed even after 700 h on stream. To the best of our knowledge, this is the first time a stannosilicate with a hierarchical BEA framework has been prepared, and the first evidence of cyclododecanone valorisation with stannosilicate catalysts.

Results and discussion

Generation of hierarchical zeolite beta

Our typical solid-state stannation methodology involves the remetallation of dealuminated (deAl-) β with Sn(II) acetate (Fig. 1). Accordingly, we first focused upon the desilication (deSi) of a pre-dealuminated (deAl) sample of H-β (denoted [deAl,deSi]-β), which was previous prepared by dealumination in HNO_3. We note here that for materials with multiple pre-treatment steps, the nomenclature used follows the order of treatment *i.e.* [deAl,deSi]-β indicates dealumination, followed by desilication. The subsequent desilication protocol employed was based on a modified protocol published by the group of Perez-Ramirez.[34] The optimised protocol involves treatment of the dealuminated solid in an aqueous solution of NaOH (0.2 M) for 0.5 h at 45 °C. Although only minor changes to the textural properties of H-β were observed after the first step *i.e.* dealumination (Table 1, Entry 2), desilication of the already dealuminated material ([deAl,deSi]-β) resulted in complete structural collapse, as evidenced by the porosimetry data (Table 1, Entry 3) and XRD analysis (Fig. 2c). Clearly, the presence of framework Al in the zeolite is essential for desilication to proceed without complete destruction of the framework, in line with previous research.[41]

We subsequently reversed our preparation procedure, and first desilicated the parent zeolite directly (deSi-β, Table 1 Entry 4). The desilication procedure employed leads to several changes in the properties of the parent zeolite. Substantial increases in BET surface area (S_{BET}), external surface area (S_{ext}), and total pore volume (V_{total}) are accompanied by decreased micropore surface area (S_{micro}), and micropore volume (V_{micro}). More crucially, however, is the retained crystalline structure (Fig. 2) and the substantial increase in mesopore volume (V_{meso}) following the desilication procedure. Having generated a clearly hierarchical structure, we subsequently dealuminated the material in line with our previous work, in order to generate the

Table 1 Textural properties of sample used in this work

Sample	S_{BET}[a] ($m^2\ g^{-1}$)	$S_{external}$[b] ($m^2\ g^{-1}$)	S_{micro}[b] ($m^2\ g^{-1}$)	V_{total}[c] ($cm^3\ g^{-1}$)	V_{micro}[b] ($cm^3\ g^{-1}$)	V_{meso}[d] ($cm^3\ g^{-1}$)
Parent H-β	498	61	437	0.35	0.23	0.11
deAl-β	541	124	417	0.53	0.23	0.22
[deAl,deSi]-β	243	197	47	0.40	0.0	0.4
deSi-β	805	483	323	0.95	0.19	0.76
[deSi,deAl]-β (h*β)	691	458	233	0.84	0.15	0.61
2Sn-h*β	614	356	259	0.67	0.15	0.52
2Sn-β	528	115	412	0.42	0.23	0.20
2Sn-MCM-41	832	832	0	0.85	0	0.85

[a] Brunauer–Emmett–Teller surface area (S_{BET}) was calculated from BET method. [b] External and micropore surface area (S_{ext} and S_{micro}) and micropore volume (V_{micro}) derived from the *t*-plot method. [c] Total pore volume (V_{total}) was evaluated at $P/P_0 = 0.99$. [d] Meso pore volume (V_{meso}) was calculated according to $V_T - V_{micro}$.

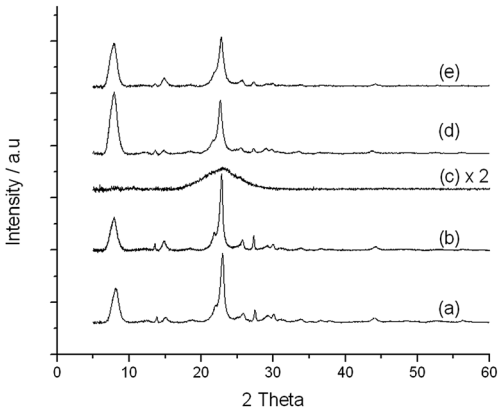

Fig. 2 XRD patterns for (a) commercial zeolite β, (b) deAl-β, (c) [deAl,deSi]-β, (d) [deSi,deAl]-β (h*β) and (e) 2Sn-h*β.

vacant framework sites required for the incorporation of tin ([deSi,deAl]-β, Table 1 Entry 5).

Despite the dealumination protocol being able to induce some mesopore formation and increasing S_{BET} and S_{ext} on its own (Table 1, Entry 2), dealumination of the desilicated structure ([deSi,deAl]-β, henceforth h*β) leads to minor decreases in each of these parameters (Table 1, Entry 5) compared to desilication alone (Table 1, Entry 4). The complete absence of Al from the dealuminated material confirms that extra-framework Al species are not present and are therefore not partially blocking the pores (Table S1†). Accordingly, we attribute this unexpected result to a slight relaxation of the framework upon removal of the isomorphously substituted framework atoms.

Physical adsorption in micropores, such as those found in the zeolites in this study, occurs at relative pressures substantially lower than in case of adsorption in mesopores. We note, therefore, that adsorption measurements with N_2 at 77.4 K do not directly provide information on the microporosity of the samples. However, it remains an extremely useful methodology for gaining insight into the mesoporosity of the materials, which is clearly a key parameter for hierarchical materials. Type I isotherms, as observed for purely microporous zeolites, exhibit a large plateau region at relative pressures above values of approximately 0.1, whereas mesoporous materials, which display Type IV character, typically experience adsorption at intermediate relative values. Although missing the low relative pressure region (*vide supra*), the N_2 adsorption isotherm obtained for Al-β is clearly reminiscent of a Type I isotherm, and Type IV character is clearly gained following dealumination (deAl-β, open triangles), or more extensively by the [deSi,deAl] treatment (h*β, open circles). This clearly demonstrates the formation of mesopores, which is more readily visualised from the BJH data. In line with its microporous structure, no mesopores are evident in Al-β. For deAl-β and h*β, the presence of new mesopores with pore diameters of approximately 7–8 nm are evident. These values are in excellent agreement to previous work with hierarchical zeolites.[30] The more extensive adsorption observed for h*β indicates that the extent of mesopores formation increases substantially with the added disilication step. It can also be observed that the dealumination step alone is able to introduce some minor mesoporosity, although to a substantially lower degree than desilication (Fig. 3).

Scanning Electron Microscopy analysis of the final catalysts *i.e.* hierarchical and microporous Sn-β, demonstrated that neither the deAl protocol (in the case of the microporous Sn-β) nor the [deSi,deAl] protocol (as for the hierarchical material) overly modified the zeolite crystals (Fig. 4a–c). No significant

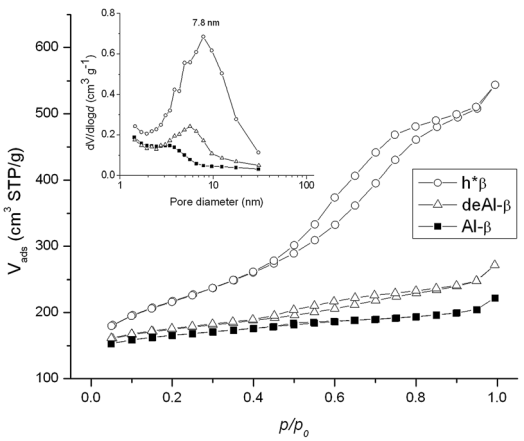

Fig. 3 Porosimetry data for (black/squares) commercial zeolite β, (hollow/triangles) deAl-β, and (hollow/circles) [deSi,deAl]-β (h*β).

changes in terms of crystal morphology or size are observed. Spherical crystals between 0.2 to 0.9 μm were maintained after the post-synthetic treatments. Although the samples experience some beam damage, preliminary TEM studies confirmed the absence of any major mesopores in deAl-β, and confirms the presence of mesopores (5–10 nm) in the h*β material. The absence of major bulk SnO_2 (*vide infra*) domains is also evident from this analysis.

Preparation and characterisation of 2Sn-h*β, following solid state stannation

Subsequently, we focused upon the solid-state incorporation of Sn(IV) into the vacant tetrahedral framework sites of h*β, according to our recently published[11] and patented solid-state stannation methodology. The preparation typically involves the dealumination of zeolite beta with HNO_3, prior to remetallation with tin. In this case, our typical solid-state stannation procedure was preceded by the desilication step (Fig. 1). In contrast to approaches whereby pre-synthesised stannosilicates are converted into hierarchical matrices, incorporating Sn post-synthetically into a pre-modified hierarchical structure ensures the presence of accessible Sn(IV) sites in the mesopores, in line with the observations of Dapsens *et al.*[37]

Tin(IV) was introduced *via* a tin(II)acetate precursor. In line with our recent work, we focused upon the preparation of materials with a high degree of site isolation, and consequently incorporated 2 wt% of Sn into the material, as this is a loading we have shown to lead to the highest levels of intrinsic activity *i.e.* TOF per Sn atom. The materials are henceforth denoted as 2Sn-β (microporous) and 2Sn-h*β (hierarchical). A multitude of spectroscopic techniques (XAS, MAS NMR, DRIFTS) were subsequently employed to verify the speciation of the incorporated Sn(IV) atoms, and to deduce whether Sn(IV) had incorporated into the vacant framework sites of h*β. A control sample of microporous 2Sn-β was also prepared, whereby 2 wt% Sn was incorporated into a dealuminated (but not desilicated) material. We have recently benchmarked the activity, selectivity and Sn site speciation of this control sample in depth.

We first employed *in situ* DRIFT spectroscopy (with CD_3CN probe) to verify the presence of Lewis acidic, framework Sn(IV) sites in both 2Sn-β and 2Sn-h*β. CD_3CN is an extremely useful probe molecule for Lewis acidic zeolites since it can interact with the framework heteroatoms,[42,43] resulting in an acid–base adduct that displays an intense absorbance at 2311 cm^{-1}. This particular feature is not observed for extra-framework Sn species nor SnO_2, and its appearance can thus confirm the presence of framework Sn(IV) atoms. As can be seen (Fig. 5A), upon dosing 2Sn-h*β with CD_3CN, two intense features are observed in the DRIFTS spectrum.[44,45] The first (2275 cm^{-1}) arises from physisorbed CD_3CN, which is readily desorbed from the sample upon heat treatment (see desorption profile, temperature increasing from top (50 °C) to bottom (200 °C)). The second feature (2311 cm^{-1}), arises from the CD_3CN molecules interacting with framework Sn(IV) atoms, and clearly demonstrates the presence of isomorphously substituted Sn atoms in our material, in excellent agreement to our prior work. The comparative spectra of purely microporous 2Sn-β are also displayed in Fig. 5B. The presence of Lewis acidic Sn heteroatoms is also evident in this material. Similar observations are found in the DRIFT spectra of CD_3CN-dosed 2Sn-MCM-41 (Fig. S3†).

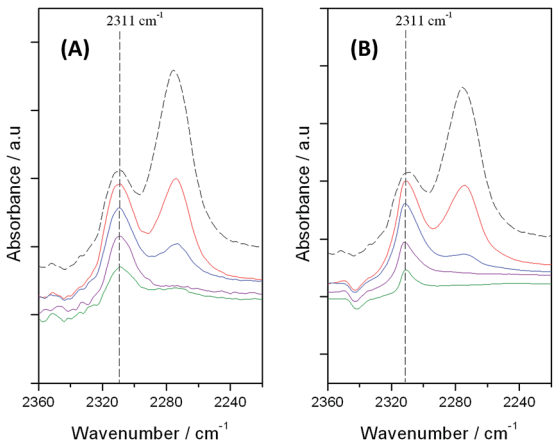

Fig. 5 *In situ* DRIFTS spectra of (A) 2Sn-h*β, and (B) 2Sn-β, following (dashed) 10 minute treatment with CD_3CN at room temperature. Various desorption temperatures (50 (red), 100 (blue), 150 (purple) and 200 °C (green)) are also displayed.

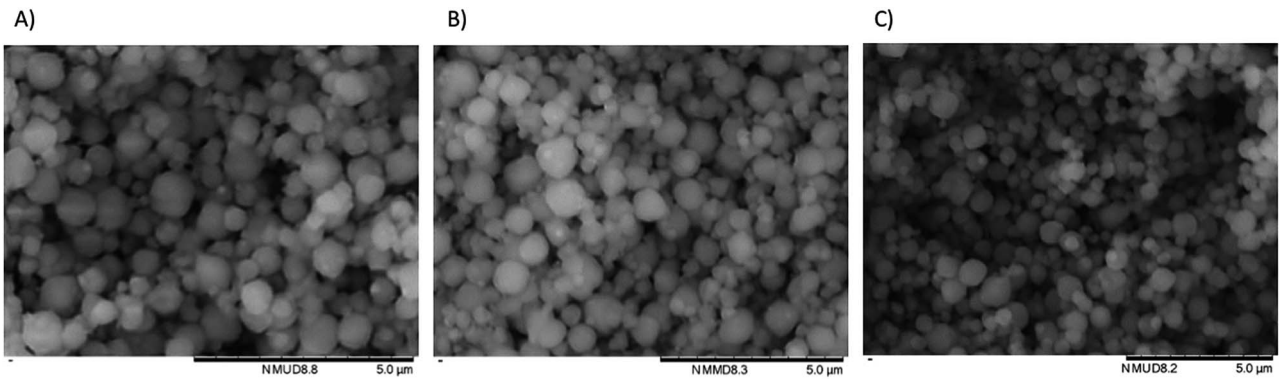

Fig. 4 SEM images of (A) commercial zeolite β, (B) 2Sn-β, and (C) 2Sn-h*β.

Although there are some minor differences in absorbance intensity and desorption rate for both of these samples, DRIFT spectroscopy is not sufficiently quantitative to differentiate between the total number of Lewis acidic (framework) and spectator sites (extra-framework) in each of these materials. Accordingly, we turned our attention to spectroscopic techniques that provide more detailed insight of the Sn site speciation, such as X-ray Absorption Spectroscopy (XAS) and Magic Angle Spinning (MAS) NMR.

Despite the low S/N ratio (materials were prepared with naturally abundant ^{118}Sn), the ambient temperature and pressure MAS NMR spectra of 2Sn-β and 2Sn-h*β primarily consists of an intense resonance at −688 ppm, which is indicative of framework Sn(IV) species in their hydrated state, in excellent agreement with our recent work (Fig. 6). The absence of a substantial resonance at −602 ppm in the spectrum of 2Sn-β indicates that extra-framework Sn species are a very minor component of this catalytic material. The presence of a shoulder at −602 ppm does, however, indicate that a minor quantity of extra-framework Sn is present in this material, both in line with our previous study,[11] and that of Bare and co-workers focusing on conventional *i.e.* hydrothermally prepared, Sn-β.[46]

In good agreement to the spectrum of 2Sn-β, the MAS NMR spectrum of 2Sn-h*β is also dominated by a resonance at −688 ppm, indicative of Sn being primarily present within the zeolite framework.[47–49] In contrast to the spectrum of 2Sn-β, however, at least one additional resonance at −591 ppm is present. The chemical shift of this resonance overlaps with the resonance observed for extra-framework Sn sites, such as SnO_2 (−602 ppm), but with a +11 ppm shift. This shift, coupled with the pronounced asymmetry of the resonance, causes some ambiguity as to whether this resonance is associated with a minor contribution of extra-framework Sn species, or isolated Sn sites present in a different geometrical position or hydrated state to those typically found in Sn-β. Given the XAS analysis (*vide infra*) and the observation that a dehydration/rehydration protocol did not affect the intensity or position of this resonance, we tentatively attribute it to extra-framework Sn sites in a slightly perturbed environment. Even so, the MAS NMR data obtained for the hierarchical material is in excellent agreement to that obtained for our microporous Sn-β at similar metal loadings, and indicates that Sn(IV) is primarily present in the zeolite framework.

To verify the presence of extra-framework Sn species in these samples, we also probed the Sn site speciation with X-ray Absorption Spectroscopy. Various elements of the EXAFS spectra of 2Sn-h*β and the conventional microporous analogue are shown in Fig. 7A and B. The spectra are of excellent quality up to a distance of 14 Å^{-1}. The first feature present arises from Sn–O scattering interactions, whilst the second feature (*ca.* 2.5–4 Å) arises from Sn–Sn scattering interactions, which are indicative of (i) extra-framework Sn atoms that are oligomeric or oxidic in nature, and/or (ii) Sn–Sn pairing.[44] It is clear from this analysis neither material possesses a substantial quantity of extra-framework Sn, given the relatively minor scattering intensity observed between 2.5 and 4 Å, particularly when compared to a reference sample of SnO_2. However, the intensity of the second shell region clearly differs between both the microporous and hierarchical analogues, with Sn–Sn scattering interactions clearly being more intense in the hierarchical material. We conclude that this confirms the presence of an extra-framework Sn component in the hierarchical matrix, suggesting that the modified porosity following the generation of mesopores leads to a very slight increase in difficulty for incorporating Sn into the framework successfully. This is in full agreement to the MAS NMR analysis of 2Sn-β and 2Sn-h*β.

In summary, the spectroscopic study undertaken indicates that Sn(IV) is almost exclusively incorporated into the vacant framework sites of h*β, although a non-negligible fraction of extra-framework Sn species appear to be present at very low concentrations. The fraction of extra-framework Sn appears to be somewhat larger in the hierarchical Sn-β than for purely microporous Sn-β, that the modified hierarchical topology has some impact on the solid-state stannation step. Nevertheless, the relatively low quantity of extra-framework Sn observed in both materials, as observed spectroscopically and through TEM

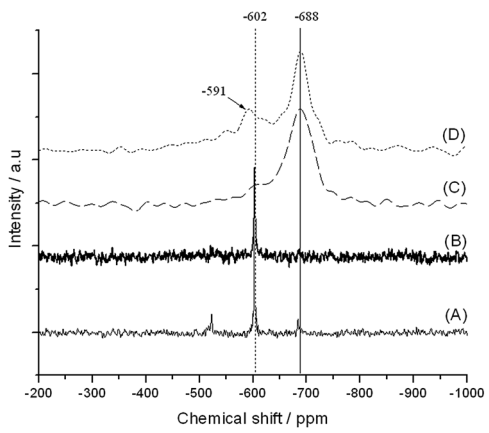

Fig. 6 MAS NMR spectra of (A) SnO_2, (B) 10% SnO_2/deAl-β (physical mixture), (C) 2Sn-β, and (D) 2Sn-h*β.

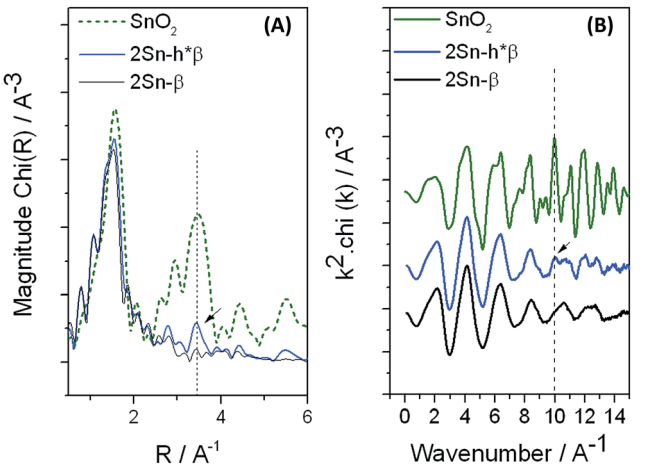

Fig. 7 (A) Magnitude of the Fourier transform spectra, and (B) EXAFS k^3-weighted *x* data, of 2Sn-β, (black) and 2Sn-h*β (blue). The corresponding spectra of SnO_2 (green dots) are also displayed.

analysis (Fig. S1†), agrees both with our previous studies,[11] and those published for conventional Sn-β, and provides us with two suitable materials from which the benefit(s) of a hierarchical topology may be studied.

Catalytic studies

To probe the catalytic properties of our hierarchical stannosilicates, particularly in reference to purely microporous Sn-β, we focused upon the Meerwein–Pondorf–Verley (MPV) transfer hydrogenation of various cyclic ketones to alcohols (Scheme 1). We chose this probe reaction for two main reasons; (i) we have recently shown it to be an excellent model reaction for Sn-β catalysis, matching the TOF trends observed for other Sn-β the isomerisation of glucose to fructose;[11] (ii) in contrast to several other Sn-β catalysed reactions (*e.g.* glucose–fructose isomerisation, BVO), the MPV process is an intermolecular reaction, which requires coordination of both the ketone substrate and the alcohol solvent. It is, therefore, a very sterically challenging reaction, and provides an excellent case study for the hierarchical materials. The activity of both zeolite materials *i.e.* 2Sn-h*β and 2Sn-β, were compared to an authentic sample of Sn-MCM-41, an amorphous but ordered, mesoporous Sn-containing silicate containing 2 wt% Sn. The characterisation of this material is provided in the ESI Fig. S2–S4.†

To fully evaluate the performance of 2Sn-h*β and 2Sn-β, and to determine the positive (or negative) impact of the hierarchical matrix, we performed the MPV transfer hydrogenation of various cyclic ketones, containing between 6 and 12 carbon atoms (*i.e.* cyclohexanone to cyclododecanone). To date, only C_6 substrates have been efficiently converted by MPV transfer hydrogenation under the mediation of purely microporous Sn-β, with diffusion limitations largely accounting for the poor activity observed for bulkier substrates. Indeed, whilst cyclohexanone (kinetic diameter, 6.0 Å, relative diameter 1.0) is on the borderline of being able to freely diffuse in the pores of zeolite beta (free diffusion limit of a sphere, 5.95 Å),[50] cyclooctanone (relative diameter 1.1) and cyclododecanone (1.4) should be too large to freely diffuse through the micropores of zeolite beta (ESI, Fig. S5†), even before the need for solvent molecule coordination is considered (*vide supra*). The three substrates therefore provide a useful span of molecular sizes to truly evaluate the performance of the hierarchical material. We first focused upon the MPV transfer hydrogenation of cyclohexanone (Fig. 8A), which can be effectively catalysed by purely microporous Sn-β. The initial reaction conditions chosen for this reaction were identical to those recently published by our team.[11] Initial rate data was used to accurately compare the intrinsic activity of each catalytic material without excessive influence from (product induced) deactivation.

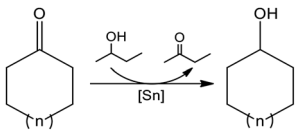

Scheme 1 Generalised scheme for the MPV transfer hydrogenation of various ketones.

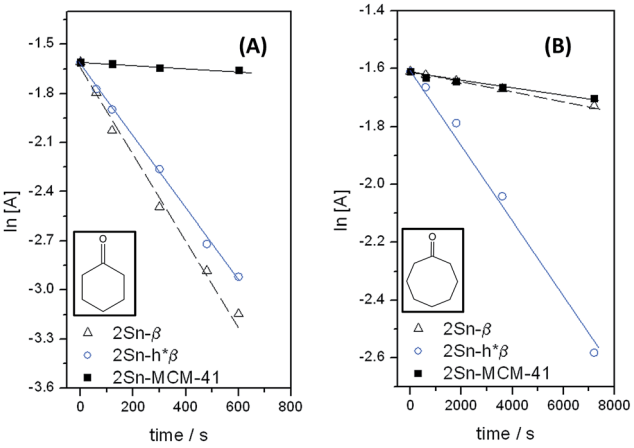

Fig. 8 Catalytic activity for 2Sn-β (open triangles), 2Sn-h*β (open circles) and 2Sn-MCM-41 (filled squares) for the MPV reduction of (A) cyclohexanone and (B) cyclooctanone.

Fig. 8 shows that the pseudo-first order rate constants for the MPV transfer hydrogenation of cyclohexanone are extremely similar for both 2Sn-β (2.5×10^{-3} s^{-1}) and 2Sn-h*β (2.2×10^{-3} s^{-1}), although there is a minor decrease in activity for the hierarchical material. We attribute this minor decrease in activity to the presence of additional extra-framework Sn species in this material, which decreases the relative amount of active Sn per gram of catalyst. Nevertheless, the comparable catalytic rates obtained over these two materials indicates that (a) the generation of a hierarchical structure does not excessively impact the intrinsic activity of the isomorphously substituted Sn atoms within the matrix, a key result given the decreased intrinsic activity observed in other reports (*vide supra*), and (b) that increased micropore accessibility is not essential for enhanced catalytic rates to be observed for C_6 substrates. This is in line with our observation that the C_6 reaction experiences no internal mass transfer limitations (Fig. 9).

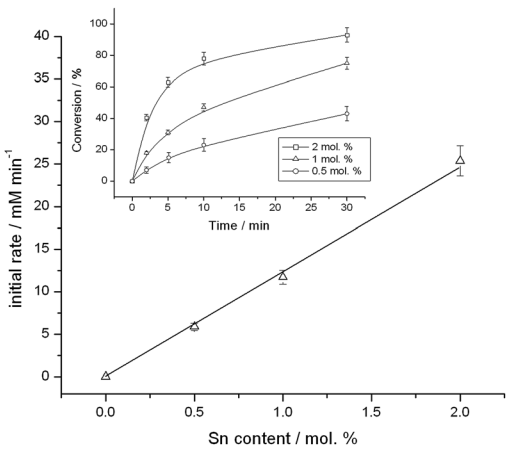

Fig. 9 Catalytic activity of 2Sn-β for the MPV hydrogenation of cyclohexanone as a function of catalyst loading. Sn content was varied by changing the mass of 2Sn-β present in the reactor. Both the initial rate data (main figure) and the time online analysis as a function of Sn content within the reactor (inset) are presented.

However, as the size of the cyclic ring is increased beyond six carbon atoms, the significant advantages of the hierarchical BEA framework become apparent. For the MPV reduction of cyclooctanone (Fig. 8B), the hierarchical material is by far the most active catalyst, demonstrating a catalytic rate (1.4×10^{-4} s^{-1}) over one order of magnitude greater than that observed over the conventional microporous analogue (1.6×10^{-5} s^{-1}), and also the mesoporous material 2Sn-MCM-41 (1.2×10^{-5} s^{-1}). Increasing the carbon chain length of the ketone substrate is highly detrimental to catalysis in the microporous analogue, demonstrating that pore size limitations are a major disadvantage of the conventional BEA framework structure when bulkier substrates are undergoing study. To further evaluate the performance of these three materials, we also examined the comparative performance of each catalyst as a function of conversion and selectivity against time. The superior performance of the hierarchical analogue for the larger substrate is clearly evident, particularly at extended reaction times (Table 2). In line with previous research, neither deAl-β, nor SnO_2 dispersed upon deAl-β behave as suitable catalysts for these reactions.

To further probe this, we also explored the MPV reduction of cyclododecanone (Fig. 10A). In this case, the catalytic rate of 2Sn-h*β (1.0×10^{-4} s^{-1}) is again over one order of magnitude greater than that observed over the microporous material (8.5×10^{-6} s^{-1}) and 2Sn-MCM-41 (6.9×10^{-6} s^{-1}). To the best of our knowledge, this is the first time that an efficient heterogeneous catalyst for the catalytic valorisation of cyclododecanone in the liquid phase has been reported, a key result given that this substrate is a precursor to laurolactam and hence, polyamide 12. This clearly demonstrates that the presence of a hierarchical structure significantly improves the general applicability of Sn-β, is extremely beneficial to Sn-mediated catalysis in general.

In all cases, the ordered mesoporous analogue, Sn-MCM-41, is the least active catalyst for these catalytic transformations, although its performance relative to microporous Sn-β improves substantially as the carbon chain length is increased. This lower activity of 2Sn-MCM-41 relative to the hierarchical material is likely due to the lower levels of Lewis acidity exhibited by heteroatoms when buried in the amorphous walls. We note that for both zeolitic materials, the selectivity to the primary MPV product (alcohol) remains largely constant at above 90% regardless of the size of the substrate. However, the selectivity observed for 2Sn-MCM-41 is

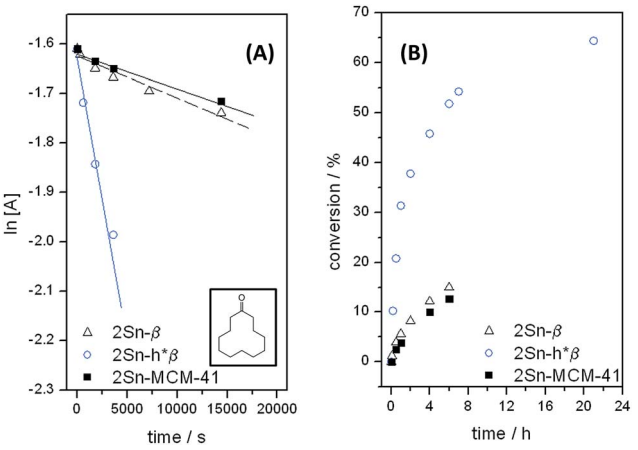

Fig. 10 (A) Initial rate data for 2Sn-β (open triangles), 2Sn-h*β (open circles) and 2Sn-MCM-41 (filled squares) for the MPV reduction of cyclododecanone, and (B) extended time online profile for the same reactions.

substantially lower, typically <50%, thus indicating the further favourability of the hierarchical material over the purely mesoporous analogue. At this time, we also draw attention to surprising activity exhibited by microporous Sn-β for the transfer hydrogenation of cyclododecanone (Fig. 10B). The conversion of this bulky substrate by this microporous material indicates that a certain fraction of Sn-β catalysis must occur on the external surface of the material, potentially as a consequence of external enrichment of the zeolite crystals, which is known to occur for these materials.[51]

Deactivation studies

Operational lifetime is a critical, but often overlooked, key performance indicator a heterogeneous catalyst.[52] Due to their microporous structure, zeolites such as Sn-β are particularly prone to some deactivation events, such as fouling, which can significant impact their commercial feasibility. Some of us recently demonstrated that Sn-β possesses high levels of stability during Lewis acid catalysis (MPV transfer hydrogenation), but steadily deactivates over the course of steady state operation. Our spectroscopic and kinetic analysis revealed that product absorption and coking were largely responsible for this slow but steady decrease in catalytic activity, causing fouling *i.e.*

Table 2 Catalytic performances of microporous and hierarchical Sn-β, and Sn-MCM-41, for the MPV hydrogenation of cyclohexanone and cyclooctanone

Catalyst	Cyclohexanone converted (cyclohexanol selectivity)[a]	Cyclooctanone converted (cyclooctanol selectivity)[b]
2Sn-β	97.5 (>95)	17.9 (90)
2Sn-h*β	93.9 (>95)	83.4 (94)
2Sn-MCM-41	8.2 (49)	12.5 (45)
deAl-β	0.8 (26)	1.1 (29)
$2SnO_2$/deAl-β	1.2 (10)	1.0 (24)

[a] Reaction conditions: cyclohexanone (0.2 M) in 2-butanol, 10 mL; 100 °C; 1.0 mol% Sn relative to CyO; 750 rpm; 30 minutes. [b] Reaction conditions: cyclooctanone (0.2 M) in 2-butanol (0.2 M), 10 mL; 100 °C; 1.0 mol% Sn relative to cyclooctanone; 750 rpm; 240 minutes.

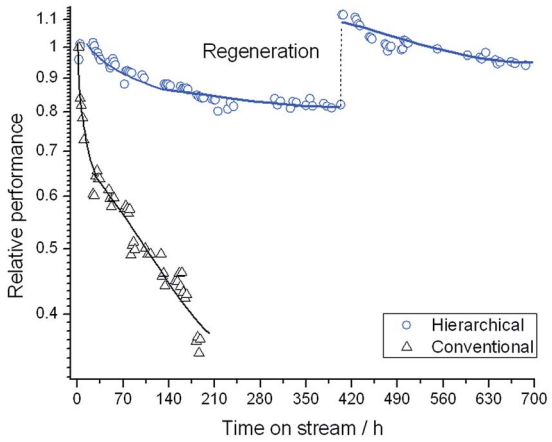

Fig. 11 Catalytic activity for 2Sn-β and 2Sn-h*β for the MPV reduction of cyclohexanone in the continuous regime.

blocking, of the micropores.[16] At this stage, we hypothesised that the improved diffusional properties of the hierarchical matrix would not only allow us to study new reactions with bulky substrates, but may also lead to decreased rates of deactivation through fouling. Consequently, we examined the steady state activity of both 2Sn-h*β and 2Sn-β for the MPV transfer hydrogenation of cyclohexanone in continuous flow. Details of our reactor are described in the ESI.†

Fig. 11 demonstrates the steady state activity of 2Sn-h*β and 2Sn-β for the MPV transfer hydrogenation of cyclohexanone over a 700 h period. The contact time for each catalyst was optimised so that similar levels of conversion (80% for 2Sn-h*β and 92% for 2Sn-β) were achieved, in order to allow accurate comparison of lifetime. As can be seen, the hierarchical analogue possess substantially improved lifetime compared to the microporous analogue. Whereas the conversion obtained over 2Sn-β decreases from 92% to 33% over a 200 h period, 2Sn-h*β retains over 80% of its original activity over 420 h on stream. With a single regeneration procedure under the conditions employed during the final calcination step (3 h, 550 °C, 60 mL min^{-1} air), 2Sn-h*β is able to catalyse the MPV reaction at >80% of its initial activity for over 700 h on stream, a remarkable improvement in long-term stability. Although periodic regeneration can also restore activity of 2Sn-β, increasing the time between essential regenerations provides added benefits for both reactor design and process economics. We note here that both the selectivity to CyOH and the carbon balance remained >95% throughout for both catalysts during steady state operation.

Conclusions

Lewis acidic zeolites have rapidly emerged as unique heterogeneous catalysts for a range of sustainable liquid phase, catalytic applications. However their microporous structure means that they lack general applicability (typically they may only be used for reactions involving small to medium sized substrates), and makes them particularly prone to deactivation through fouling. In this manuscript, we show that hierarchically porous BEA stannosilicates are able to mediate the catalytic conversion of bulky ketone substrates that purely microporous analogues are unable to catalyse. Deactivation studies in the continuous regime also demonstrate the exceptional stability of hierarchical Sn-β compared to purely microporous Sn-β, with limited (<20%) activity loss observed over 700 h on stream. In contrast, microporous Sn-β lost ±70% activity in only 200 h on stream. To the best of our knowledge, this is the first time a stannosilicate with a hierarchical BEA topology has been prepared, the first evidence of condensed phase cyclododecanone valorisation with stannosilicates, and the first full study of condensed phase deactivation kinetics for hierarchical zeolite materials.

Experimental

Catalyst synthesis

Commercial zeolite Al-β (Zeolyst, NH_4-form, $SiO_2/Al_2O_3 = 38$) was dealuminated by treatment in HNO_3 solution (13 M HNO_3, 100 °C, 20 h, 20 mL g^{-1} zeolite). The dealuminated powder was washed extensively with water (±500 mL g^{-1} catalyst), and dried overnight at 110 °C. Desilicated-dealuminated zeolite β ([deSi,-deAl]-β, referred to as h*β throughout the manuscript) was prepared as follows: commercial Al-β zeolite (CP814E, NH_4-form, $SiO_2/Al_2O_3 = 38$, Zeolyst International) was first converted into protonic form by calcination in static air at 550 °C (5 °C min^{-1}) for 5 h. The H-form zeolite was subsequently suspended in an aqueous solution of NaOH (0.2 M, 318 K, 0.5 h, 30 mL g^{-1} zeolite) to obtain a desilicated zeolite β (deSi-β). The reaction was stopped immediately by cooling the container in an ice bath. The remaining solid product was filtered, thoroughly washed with deionized water until neutral pH was attained, and finally dried at 373 K overnight. Subsequently, deSi-β was dealuminated following the same procedure described above. After filtering and drying the sample, the sample was reconverted into NH_4-form *via* ion exchange in a solution of NH_4NO_3 (1 M, 2 h, 85 °C, 30 mL solution per g (catalyst)).

Solid-state stannation of both dealuminated zeolite β (deAl-β) and [deSi,deAl]-β (h*β) was performed the procedure reported in ref. 11 and 53, by grinding the appropriate amount of tin(II) acetate with the necessary amount of dealuminated or desilicated-dealuminated zeolite for 10 minutes in a pestle and mortar. Following this procedure, the sample was heated in a combustion furnace (Carbolite MTF12/38/400) to 550 °C (10 °C min^{-1}) first in a flow of N_2 (3 h) and subsequently air (3 h) for a total dwell time of 6 h. Gas flow rates of 60 mL min^{-1} were employed at all times.

Catalyst characterisation

A PANalytical X'PertPRO X-ray diffractometer was employed for powder XRD analysis. A CuKα radiation source (40 kV and 30 mA) was utilised. Diffraction patterns were recorded between 5–55° 2θ (step size 0.0167°, time/step = 150 s, total time = 1 h). Porosimetry measurements were performed on a Quantachrome Autosorb, and samples were degassed prior to use (277 °C, 6 h). Adsorption isotherms were obtained at 77 K and various

analysis methods were employed (see Table 1). SEM Images of the catalysts were obtained using a Hitachi TM3030Plus, at 15 kV and at EDX observation conditions. The EDX tool was utilised to analyse the elemental composition and distribution. A Bruker Tensor spectrometer equipped with a Harrick praying mantis cell was utilised for DRIFT measurements. Spectra were recorded between 4000–650 cm^{-1} at a resolution of 2 cm^{-1}. CD_3CN measurements were performed on pre-treated zeolite powders (550 °C, 1 h under flowing air, 60 mL min^{-1}) according to the method described in ref. 10. MAS NMR experiments were performed at Durham University through the EPSRC UK National Solid-state NMR Service. Samples were measured under conditions identical to those reported by Bermejo-Deval *et al.*,[47] and Hammond and co-workers.[11] Sn K-edge XAS data was collected by the methods described in detail elsewhere.[11]

Kinetic evaluation and analytical methods

MPV reactions with cyclohexanone were performed in a 100 mL round bottom flask equipped with a reflux condenser, which was thermostatically controlled by immersion in a silicon oil bath. The vessel was charged with a 10 mL solution of cyclohexanone in 2-butanol (0.2 M), which also contained an internal standard (biphenyl, 0.01 M), and was subsequently heated to the desired temperature (100 °C internal temperature). The reaction was initiated by addition of an appropriate amount of catalyst, corresponding to 1 mol% Sn relative to cyclohexanone. The solution was stirred at ±750 rpm with an oval magnetic stirrer bar. MPV reactions with cyclooctanone were performed with the same methodology and conditions. MPV reactions with cyclododecanone were performed in a 15 mL thick walled glass reactor, which was thermostatically controlled by immersion in a silicon oil bath. The vessel was charged with a 5 mL solution of cyclododecanone in 2-butanol (0.2 M), which also contained an internal standard (biphenyl, 0.01 M). The appropriate amount of catalyst, corresponding to 2.5 mol% Sn relative to cyclododecanone, was also added. The reactor was subsequently heated to the desired temperature (130 °C internal temperature), and the reaction was initiated by stirring at ±750 rpm with an oval magnetic stirrer bar. Aliquots of both reaction solutions were taken periodically for analysis, and were centrifuged prior to injection into a GC (Agilent 7820, 25m CP-Wax 52 CB). Reactants were quantified against a biphenyl internal standard. Continuous flow experiments were performed as described in the ESI.†

Acknowledgements

CH gratefully appreciates the support of The Royal Society for the provision of a University Research Fellowship (UF140207) and further research funding (RG140754). AA-N is indebted to Al-Qadisiya University (Iraq) for the provision of a PhD scholarship. KY wishes to thank the Catalysis CDT for the PhD scholarship. Dr David Apperley, Dr Fraser Markwell and Dr Eric Hughes of the ESPRC UK National Solid-state NMR Service at Durham University are thanked for performing the MAS NMR experiments, and for useful discussions. Dr Peter Wells (University College London/UK Catalysis Hub) is thanked for measurement of the XAS spectra and for useful discussions. Diamond Light Source and the Research Complex at Harwell are thanked for the provision of beamtime (SP8071). Dr Nikolaos Dimitratos is thanked for continued support and discussion.

References

1 Y. Roman-Leshkov and M. E. Davis, *ACS Catal.*, 2011, **1**, 1566–1588.
2 P. Y. Dapsens, C. Mondelli, B. T. Kusema, R. Verel and J. Perez-Ramirez, *Green Chem.*, 2014, **16**, 1176–1186.
3 P. Y. Dapsens, C. Mondelli and J. P. Ramirez, *Chem. Soc. Rev.*, 2015, **44**, 7015–7430.
4 M. Moliner, *Dalton Trans.*, 2013, **43**, 4197–4208.
5 A. Corma, L. T. Nemeth, M. Renz and S. Valencia, *Nature*, 2001, **412**, 423–425.
6 C. Hammond, S. Conrad and I. Hermans, *Angew. Chem., Int. Ed.*, 2012, **51**, 11736–11739.
7 Z. Kang, X. Zhang, H. Liu, J. Qiu and K. L. Yeung, *Chem. Eng. J.*, 2013, **218**, 425–432.
8 A. Corma, M. E. Domine, L. Nemeth and S. Valencia, *J. Am. Chem. Soc.*, 2002, **124**, 3194–3195.
9 A. Corma, M. E. Domine and S. Valencia, *J. Catal.*, 2003, **215**, 294–304.
10 P. Wolf, C. Hammond and I. Hermans, *Dalton Trans.*, 2014, **43**, 4514–4519.
11 C. Hammond, D. Padovan, A. Al-Nayili, P. P. Wells, E. K. Gibson and N. Dimitratos, *ChemCatChem*, 2015, **7**, 3322–3332.
12 J. Dijkmans, D. Gabriels, M. Dusselier, F. de Clippel, P. Vanelderen, K. Houthoofd, A. Malfliet, Y. Pontikes and B. F. Sels, *Green Chem.*, 2013, **15**, 2777–2785.
13 R. Bermejo-Deval, M. Orazov, R. Gounder, S. Hwang and M. E. Davis, *ACS Catal.*, 2014, **4**, 2288–2297.
14 Y. R. Leshkov, M. Moliner, J. A. Labinger and M. E. Davis, *Angew. Chem., Int. Ed.*, 2010, **49**, 8954–8957.
15 M. Moliner, Y. R. Leshkov and M. E. Davis, *Proc. Natl. Acad. Sci. U. S. A.*, 2010, **107**, 6164–6168.
16 D. Padovan, M. S. Grasina, C. Parsons and C. Hammond, 2015, submitted manuscript.
17 J. Jiang, J. Yu and A. Corma, *Angew. Chem., Int. Ed.*, 2010, **49**, 3120–3145.
18 C. C. Freyhardt, M. Tsapatsis, R. F. Lobo, K. J. Balkus Jr and M. E. Davis, *Nature*, 1996, **391**, 295–298.
19 A. Corma, M. J. Diaz-Cabañas, J. Martinez-Triguero, F. Rey and J. Rius, *Nature*, 2002, **418**, 514–517.
20 C. Perego and R. Millini, *Chem. Soc. Rev.*, 2010, **42**, 3956–3976.
21 P. S. Niphadkar, A. C. Garade, R. K. Jha, C. V. Rode and P. N. Joshi, *Microporous Mesoporous Mater.*, 2010, **136**, 115–125.
22 L. Tosheva and V. P. Valtchev, *Chem. Mater.*, 2005, **17**, 2494–2513.
23 M. Choi, K. Na, J. Kim, Y. Sakamoto, O. Terasaki and R. Ryoo, *Nature*, 2009, **461**, 246–249.

24 K. Na, C. Jo, K. Kim, K. Cho, J. Jung, Y. Seo, R. J. Messinger, B. F. Chmelka and R. Ryoo, *Science*, 2011, **333**, 328–332.
25 A. Corma, V. Fornes, S. B. Pergher, T. L. M. Maesen and J. G. Buglass, *Nature*, 1998, **396**, 353–356.
26 L. Ren, Q. Guo, P. Kumar, M. Orazov, D. Xu, S. M. Alhassan, K. A. Mkhoyan, M. E. Davis and M. Tsapatsis, *Angew. Chem., Int. Ed.*, 2015, **54**, 10848–10851.
27 X. Ouyang, S.-J. Hwang, D. Xie, T. Rea, S. I. Zones and A. Katz, *ACS Catal.*, 2015, **5**, 3108–3119.
28 H. Y. Luo, L. Bui, W. R. Gunther, E. Min and Y. Roman-Leshkov, *ACS Catal.*, 2012, **2**, 2695–2699.
29 K. Li, J. Valla and J. Garcia-Martinez, *ChemCatChem*, 2014, **6**, 46–66.
30 J. Perez-Ramirez, C. H. Christensen, K. Egleblad, C. H. Christensen and J. C. Groen, *Chem. Soc. Rev.*, 2008, **37**, 2530–2542.
31 M. Hartmann, *Angew. Chem., Int. Ed.*, 2004, **43**, 5880–5882.
32 M. S. Holm, E. Taaring, K. Egeblad and C. H. Christensen, *Catal. Today*, 2011, **168**, 3–16.
33 T. C. Keller, J. Arras, S. Wershofen and J. Perez-Ramírez, *ACS Catal.*, 2015, **5**, 734–743.
34 J. C. Groen, L. A. A. Peffer, J. A. Moulijn and J. Perez-Ramirez, *Microporous Mesoporous Mater.*, 2004, **69**, 29–34.
35 M. S. Holm, M. K. Hansen and C. H. Christensen, *Eur. J. Inorg. Chem.*, 2009, 1194–1198.
36 L. Sommer, D. Mores, S. Svelle, M. Stöcker, B. M. Weckhuysen and U. Olsbye, *Microporous Mesoporous Mater.*, 2010, **132**, 384–394.
37 P. Y. Dapsens, C. Mondelli, J. Jagielski, R. Hauert and J. Pérez-Ramírez, *Catal. Sci. Technol.*, 2014, **4**, 2302–2311.
38 H. J. Cho, P. Dornath and W. Fan, *ACS Catal.*, 2014, **4**, 2029–2037.
39 J. C. Groen, S. Abello, L. A. Villaescusa and J. Perez-Ramirez, *Microporous Mesoporous Mater.*, 2008, **114**, 93–102.
40 J. Jin, X. Ye, Y. Li, Y. Wang, L. Li, J. Gu, W. Zhao and J. Shi, *Dalton Trans.*, 2014, **43**, 8196–8204.
41 J. C. Groen, L. A. A. Peffer, J. A. Moulijn and J. Perez-Ramirez, *Chem.–Eur. J.*, 2005, **11**, 4983–4994.
42 M. Boronat, P. Concepcion, A. Corma, M. Renz and S. Valencia, *J. Catal.*, 2005, **234**, 111–118.
43 S. Roy, K. Bakhmutsky, E. Mahmoud, R. F. Lobo and R. J. Gorte, *ACS Catal.*, 2013, **3**, 573–580.
44 A. G. Pelmenschikov, R. A. V. Santen, G. J. Pnchen and E. Meijer, *J. Phys. Chem. B*, 1993, **97**, 11071–11074.
45 J. Chen, J. M. Thomas and G. Sankar, *J. Chem. Soc., Faraday Trans.*, 1994, **90**, 3455–3459.
46 S. R. Bare, S. D. Kelly, W. Sinkler, J. J. Low, F. S. Modica, S. Valencia, A. Corma and L. T. Nemeth, *J. Am. Chem. Soc.*, 2005, **127**, 12924–12932.
47 R. Bermejo-Deval, R. Gounder and M. E. Davis, *ACS Catal.*, 2012, **2**, 2705–2713.
48 R. Bermejo-Deval, M. Orazov, R. Gounder, S.-J. Hwang and M. E. Davis, *ACS Catal.*, 2014, **4**, 2288–2297.
49 W. R. Gunther, V. K. Michaelis, M. A. Caporini, R. G. Griffin and Y. Roman-Leshkov, *J. Am. Chem. Soc.*, 2014, **136**, 6219–6222.
50 C. Baerlocher and L. B. McCusker, *Database of Zeolite Structures*, 2015, http://www.iza-structure.org/databases/.
51 S. Tolberg, A. Katerinopolou, D. D. Falcone, I. Sadaba, C. M. Osmundsen, R. J. Davis, E. Taarning, P. Fristrup and M. S. Holm, *J. Mater. Chem. A*, 2014, **2**, 20252–20262.
52 I. Sádaba, M. L. Granados, A. Riisager and E. Taarning, *Green Chem.*, 2015, **17**, 4133–4145.
53 A. Parvulscu, U. Müller, J. H. Teles, N. Vautravers, G. Uhl, I. Hermans, P. Wolf and C. Hammond, WO 2015/067654 A1, 2015.

